Catalysis Today 166 (2011) 2–9

Contents lists available at ScienceDirect

Catalysis Today

journal homepage: www.elsevier.com/locate/cattod

Novel Au–TiC catalysts for CO oxidation and desulfurization processes

José A. Rodriguez[a,*], Ping Liu[a], Yoshiro Takahashi[b], Francesc Viñes[c,d], Leticia Feria[d], Elizabeth Florez[d], Kenichi Nakamura[b], Francesc Illas[d]

[a] Department of Chemistry, Brookhaven National Laboratory, Upton, NY 11973, USA
[b] Materials and Structures Laboratory, Tokyo Institute of Technology, Yokohama 226-8503, Japan
[c] Friedrich-Alexander-Universität Erlangen-Nürnberg, Lehrstuhl für Theoretische Chemie and Interdisciplinary Center for Interface Controlled Processes, Egerlandstr. 3, D-91058 Erlangen, Germany
[d] Departament de Química Física & Institut de Química Teòrica i Computacional (IQTCUB), Universitat de Barcelona, C/Martí i Franquès 1, 08028 Barcelona, Spain

ARTICLE INFO

Article history:
Available online 5 July 2010

Keywords:
Gold
Titanium carbide
CO oxidation
Hydrodesulfurization

ABSTRACT

Recent articles dealing with the physical and chemical properties of novel Au–TiC catalysts are reviewed. High-resolution photoemission, scanning tunneling microscopy and first-principles periodic density-functional calculations were used to study the deposition of gold on a TiC(0 0 1) surface. Gold grows forming two-dimensional (very low coverage) and three-dimensional (medium and large coverage) islands on the carbide substrate. A positive shift in the binding energy of the C 1s core level is observed after the deposition of Au on TiC(0 0 1). The results of the density-functional calculations corroborate the formation of Au–C bonds. In general, the bond between Au and the TiC(0 0 1) surface exhibits very little ionic character, but there is a substantial polarization of electrons around Au that facilitates bonding of the adatoms with electron-acceptor molecules (CO, O_2, C_2H_4, SO_2, thiophene, etc.). Experimental measurements indicate that Au/TiC(0 0 1) is a very good catalysts for the oxidation of CO, the destruction of SO_2 and the hydrodesulfurization of thiophene. At temperatures below 200 K, Au/TiC(0 0 1) is able to perform the $2CO + O_2 \rightarrow 2CO_2$ reaction and the full decomposition of SO_2. Furthermore, in spite of the very poor hydrodesulfurization performance of TiC(0 0 1) or Au(1 1 1), a Au/TiC(0 0 1) surface displays a hydrodesulfurization activity higher than that of conventional Ni/MoS_x catalysts. Metal carbides are excellent supports for enhancing the chemical reactivity of gold. The Au/TiC system is more chemically active than systems generated by depositing Au nanoparticles on oxide surfaces.

1. Introduction

The carbides of the early-transition metals exhibit chemical and catalytic properties that in many aspects are very similar to those of expensive noble metals [1]. Typically, early-transition metals are very reactive elements that bond adsorbates too strongly to be useful as catalysts. These systems are not stable under a reactive chemical environment and exhibit a tendency to form compounds (oxides, nitrides, sulfides, carbides, phosphides). The inclusion of C into the lattice of an early-transition metal produces a substantial gain in stability [2]. Furthermore, in a metal carbide, the carbon atoms moderate the chemical reactivity through ensemble and ligand effects [1,2]. On one hand, the presence of the carbon atoms usually limits the number of metal atoms that can be exposed in a surface of a metal carbide (ensemble effect). On the other hand, the formation of metal-carbon bonds modifies the electronic properties of the metal (decrease in its density of states near the Fermi level; metal → carbon charge transfer) [1,2], making it less chemically active (ligand effect) and a better catalyst according to the Sabatier's principle [2]. Thus, the carbides of early-transition metals are able to catalyze the isomerization and hydrogenation of olefins [1,3], the synthesis of large hydrocarbons through the Fischer–Tropsch process [1], the conversion of methane to synthesis gas [4,5], and desulfurization reactions [1,6–15].

In this article, we review a series of studies which have recently appeared in the literature investigating the properties of novel Au–TiC catalysts for CO oxidation and desulfurization processes [16–19]. Bulk metallic gold typically exhibits a quite low chemical and catalytic activity [21,22]. Among the transition metals, gold is by far the least reactive [22], and is often referred to as the "coinage metal". However, recently, gold has become the subject of a lot of attention due to its unusual catalytic properties when dispersed on some oxide supports [23–29]. In principle, the active sites for the catalytic reactions could be located only on the supported Au particles or on the perimeter of the gold–oxide interface [23]. For several catalytic reactions, it is known that the oxide support does play a significant role in the chemical activation of the gold nanoparticles [23,24,29,30]. What happens when Au is deposited

* Corresponding author. Tel.: +1 631 344 2246; fax: +1 631 344 5815.
E-mail address: rodrigez@bnl.gov (J.A. Rodriguez).

0920-5861/$ – see front matter © 2010 Elsevier B.V. All rights reserved.
doi:10.1016/j.cattod.2010.04.051

on a substrate which has physical and chemical properties different from those of an oxide? In broad terms, the metal carbides display a unique combination of the physical properties characteristic of noble metals and ceramics [31,32]. Many early-transition metal carbides are good electrical and thermal conductors while possessing ultra-hardness and very high melting points [1,31,32]. Titanium carbide is among the most commonly used metal carbides [1,2,31,32]. It adopts a NaCl lattice structure [1,32]. The valence bands of TiC show a strong hybridization of the Ti 3d and C 2p states as expected for a covalent compound [33]. In addition, there is some degree of ionicity in the Ti–C bonds, with a charge transfer from Ti to C [33,34]. A TiC(0 0 1) surface exposes an equal number of metal and carbon atoms, and all of these centers can participate in the bonding of adsorbates (i.e. the carbon atoms are not simple spectators) [7,11,34,35]. TiC(0 0 1) binds well atomic O and S [34,35], but interacts weakly with molecules such as CO, O_2 and thiophene [19,36,37]. The addition of Au to TiC(0 0 1) dramatically enhances the chemical reactivity of the surface [16–20]. A charge polarization induced by Au ↔ C interactions produces a system which exhibits a chemical activity much larger than those found after the deposition of gold on surfaces of oxides.

This article presents an overview of studies published for the Au/TiC(0 0 1) system. It is organized as follows. The next section gives a summary of the experimental and theoretical methods used in these studies [17–20]. Then, we describe studies examining the interaction of gold with TiC(0 0 1) using synchrotron-based high-resolution photoemission, scanning tunneling microscopy (STM) and periodic density-functional (DF) calculations [17,18]. This is followed by studies focused on the adsorption of O_2 and oxidation of CO on Au/TiC(0 0 1) surfaces [20]. In the last part of the article, we end with studies of DeSOx and hydrodesulfurization processes on clean and gold-promoted TiC(0 0 1) [18,19].

2. Experimental and theoretical methods

2.1. Experimental studies

Several techniques have been used to study the physical and chemical properties of Au/TiC(0 0 1) surfaces [17,20]. The photoemission studies were performed in a conventional ultrahigh-vacuum (UHV) chamber (base pressure ~ 5×10^{-10} Torr) located at the U7A beamline of the National Synchrotron Light Source (NSLS) at Brookhaven National Laboratory [34,35]. The chamber contains a hemispherical electron energy analyzer with multichannel detection, instrumentation for low-energy electron diffraction (LEED), and a quadrupole mass spectrometer. The C 1s, S 2p and Au 4f spectra reported in Section 3 were generally recorded using a photon energy of 380 eV. The Ti 2p and O 1s spectra were acquired using photon energies of 550 and 625 eV, respectively. The overall instrumental resolution in these photoemission experiments was ~0.3 eV. The binding energy scale in the photoemission spectra was calibrated by the position of the Fermi edge in the valence region.

Additional experiments were performed at two UHV chambers (base pressure < 3×10^{-10} Torr) located at the Tokyo Institute of Technology (TIT) with capabilities for X-ray photoelectron spectroscopy (Al Kα X-ray source), LEED, Auger electron spectroscopy (AES), thermal-desorption mass spectroscopy (TDS), and scanning tunneling microscopy (STM) [18,19,34,35]. One of these UHV chambers has attached a high-pressure cell or batch reactor [19] that was used to test the hydrodesulfurization activity of the Au–TiC catalysts.

In the UHV chambers at BNL and TIT, the TiC(0 0 1) crystal was mounted and cleaned following the methodology described elsewhere [38,39]. The cleaning procedure led to a clear 1×1 diffraction pattern in LEED and no surface impurities in photoemission or XPS. The crystal growers estimated a $TiC_{0.95–0.98}$ stoichiometry for the bulk of the sample, and after cleaning our quantitative XPS results showed surfaces with essentially a Ti/C ratio of one [34,35]. For surfaces prepared in this way, images of scanning tunneling microscopy (STM) gave a square crystal lattice with terraces that were 400–550 Å wide, separated by single and double step heights. Au was vapor deposited on TiC(0 0 1) at room temperature. The flux from the metal doser was calibrated by depositing Au on a Mo(1 0 0) crystal and taking thermal-desorption spectra of the admetal [17]. O_2, SO_2 and thiophene (≥99.9% purity) were dosed into the UHV chambers through gas-capillary arrays positioned near the samples. The gas exposures are based on ion-gauge readings and are not corrected for the capillary array enhancements.

2.2. Theoretical studies

Periodic density-functional (DF) calculations, performed with the VASP or DMol^3 codes, were also used to study the physical and chemical properties of Au/TiC(0 0 1), as detailed in Refs. [17–20]. In the past, we have found that DF calculations with these codes gave very similar results for the structures of metal-carbide surfaces [33] and for the bonding geometries and adsorption energies of oxygen on carbides [36]. VASP uses a plane-wave basis set [40], while DMol^3 utilizes localized atomic orbitals with a numerical basis set [41]. The bonding energies of the adsorbates were calculated using the generalized-gradient approximation (GGA) with the revised Perdew-Burke-Ernzerhof (RPBE) functional [42] in DMol^3 and with the PW91 [43] GGA functional in VASP. Slabs of three or four atomic layers were utilized to model the metal carbide substrates [17–20]. During the DF calculations the geometries of the first layer (DMol^3) or the two first layers (VASP) of the carbide and the adsorbates were allowed to fully relax [17–20]. Using the final optimized geometries, the adsorption energies were calculated by means of the following equation:

$$E_{\text{adsorption}} = E_{\text{adsorbate/surface}} - (E_{\text{adsorbate}} + E_{\text{surface}}) \quad (1)$$

where E_{surface} is the total energy of the relaxed carbide surface, $E_{\text{adsorbate}}$ is the energy of the isolated adsorbate in the vacuum, and $E_{\text{adsorbate/surface}}$ is the energy of the TiC(0 0 1) surface with the adsorbate. A negative value of $E_{\text{adsorption}}$ denotes an exothermic process. To better understand the nature of the interactions of gold with TiC(0 0 1), the electronic structure has been analyzed through a topological analysis of the Electron Localization Function (ELF) [44] and charge distributions were estimated by the method of Bader [45].

3. Results and discussion

3.1. Interaction of gold with TiC(0 0 1)

The results of STM and XPS for Au on TiC(0 0 1) point to a lack of layer-by-layer growth, with the formation of two-dimensional (2D) and three-dimensional (3D) islands of the admetal over the carbide surface [17–19]. 3D growth has been seen for Au on TiC films [46,47]. Fig. 1 shows the distribution of heights observed with STM after depositing 0.1, 0.5 and 1.5 ML of Au on TiC(0 0 1) [18–20]. For a Au coverage of 0.1 ML, a large fraction of the Au particles exhibits a height of ~0.2 nm with respect to the carbide substrate These small particles are 2D (i.e. one single Au layer) and have a diameter below 0.6 nm [18], which would point to particles such as planar Au_4 with a diameter 0.4 nm [17]. For a Au coverage of 0.5 ML, one sees a significant increase in the average height of the Au particles. When the Au coverage is increased to 1.5 ML, the average height is larger than 1 nm and the Au particles are mainly 3D. In general, for Au coverages higher than 1 ML, one is dealing with 3D

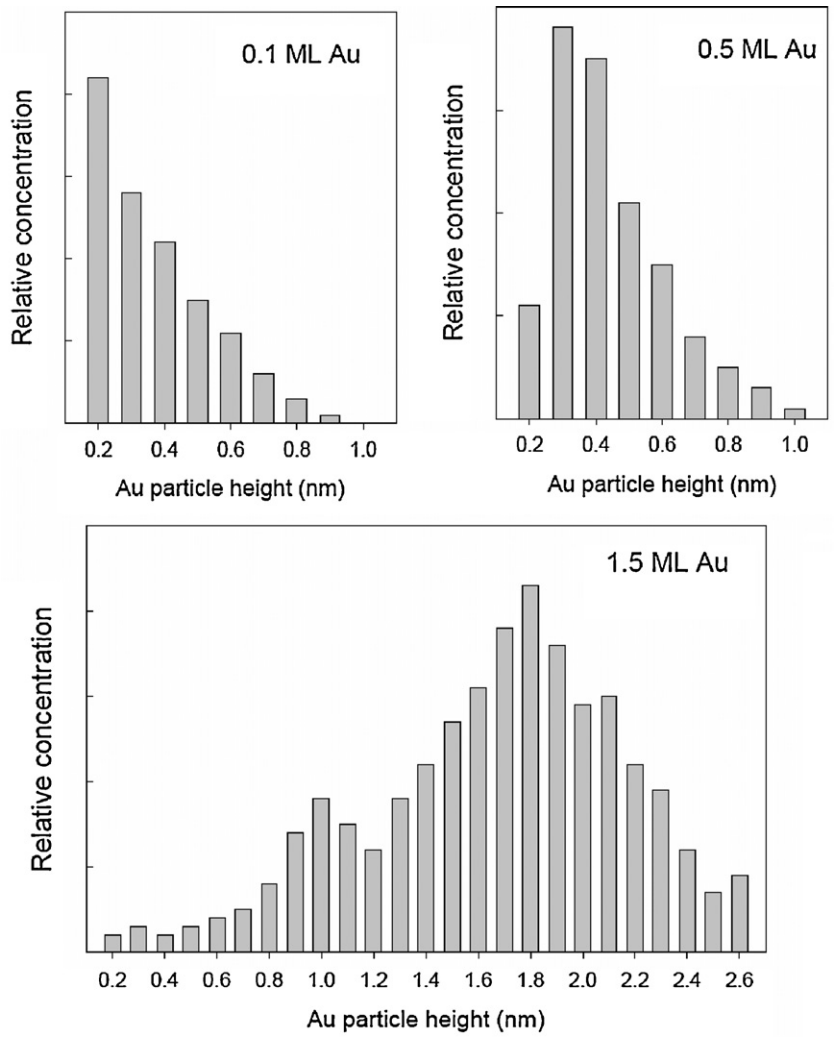

Fig. 1. Distribution of Au particle heights seen in STM images for 0.1, 0.5 and 1.5 ML of gold on TiC(0 0 1). Au was vapor deposited at 300 K and the Au/TiC(0 0 1) surfaces were annealed to 550 K before taken the STM images [18,19]. At a coverage 0.1 ML, gold is forming a significant fraction of 2D islands on the carbide substrate. For a coverage of 1.5 ML, gold mainly forms 3D islands on TiC(0 0 1).

Au particles which have sizes in the range of 1.5–3 nm [18]. As we will see below, the size of the Au particles has a dramatic effect on the chemical reactivity of the Au/TiC(0 0 1) systems.

The results of high-resolution photoemission show a strong Au ↔ TiC(0 0 1) interaction [17]. Fig. 2 displays the variation of the binding energy of the Au $4f_{7/2}$ peak as a function of gold coverage on TiC(0 0 1). At very small Au coverages, a binding energy of 84.16 eV was observed and there was a monotonic decrease up to a value of ~83.8 eV at coverages above 0.5 ML. The final value is close to that seen in our instrument for bulk metallic gold. The positive shift in the Au $4f_{7/2}$ peak at very low Au coverages could be due to a redistribution of charge around the adatoms [17]. This binding energy shift is quite clear for small Au particles in which a large fraction of the adatoms are in contact with the TiC(0 0 1) surface.

The C 1s core level of TiC(0 0 1) is affected by the adsorption of gold [17]. C 1s core level spectra recorded before and after dosing 0.3 ML of Au to TiC(0 0 1) are shown in Fig. 3. The deposition of Au induces an attenuation in the intensity and an increase of 56% in the full-width at half-maximum of the C 1s peak. In Fig. 3, the subtraction of the re-normalized spectrum "a" from spectrum "b" produces a spectrum with a C 1s peak at ~282.4 eV [17]. These features probably reflect Au–C bonding. The Au-induced shift in the C 1s features (~0.55 eV) is substantially smaller than the shifts induced by adsorption of O and S on TiC(0 0 1) (1.5–1.8 eV) [34,35]. On the

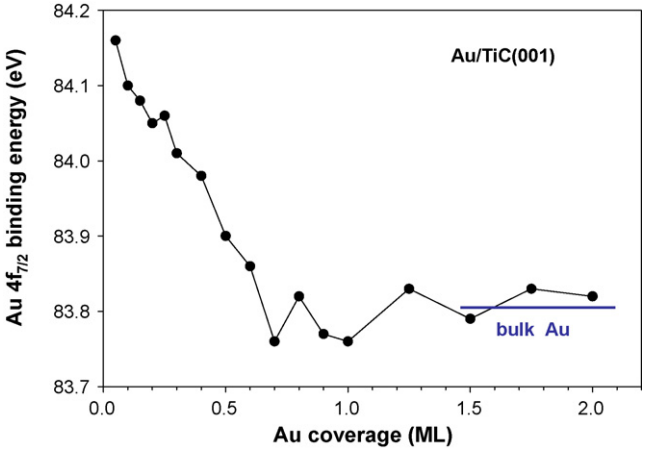

Fig. 2. Variation of the Au $4f_{7/2}$ binding energy for Au/TiC(0 0 1) as a function of Au coverage. For comparison, we also include the Au $4f_{7/2}$ binding energy measured in our instrument (83.81 eV) for bulk metallic Au [17]. The photoemission data were obtained using a photon energy of 380 eV.

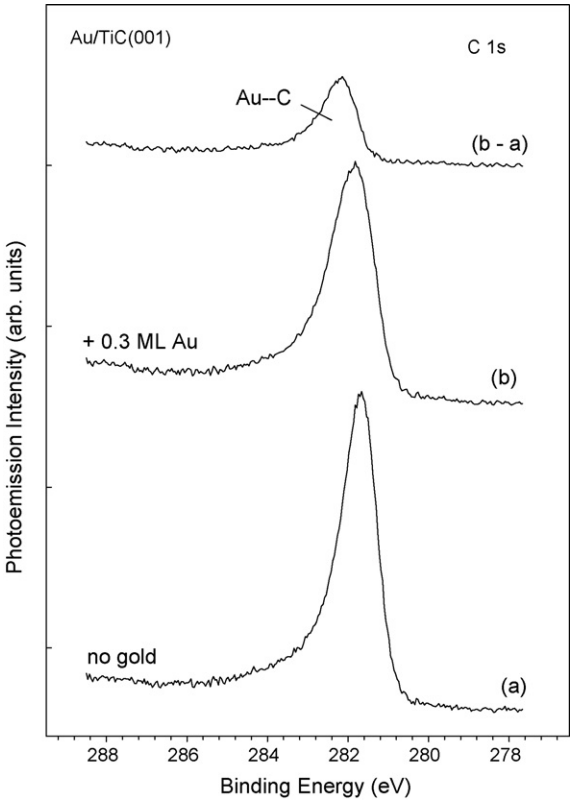

Fig. 3. C 1s core level spectra obtained before (a) and after depositing (b) on TiC(0 0 1) at 300 K. At the top of the figure, we show the subtraction of the re-normalized spectrum "a" from spectrum "b" which produces C 1s features centered at ~282.4 eV [17]. A photon energy of 380 eV was used to acquire these C 1s core level spectra.

basis of differences in electronegativity, the Au–TiC(0 0 1) bond is expected to be less ionic than the O–TiC(0 0 1) or S–TiC(0 0 1) bond and hence one also expect a smaller degree of charge transfer.

The photoemission results seem to indicate that Au prefers to interact with the C sites of TiC(0 0 1). DF calculations for gold atoms and a series of clusters (Au_2, Au_4, Au_{13}, Au_{29}) on TiC(0 0 1) confirm this hypothesis [17–19]. The strongest bonding interactions are observed when the Au atoms are above C sites, and the weakest for bonding above Ti sites [17]. Although the Au-surface bonding energies are quite significant (1.9–2.4 eV per Au atom), they are still smaller than the cohesive energies calculated for 3D gold clusters (2.5–2.7 eV) [17]. Thus, the calculations indicate that Au adatoms should form 3D aggregates, as seen in images of STM for Au/TiC(0 0 1) [18,19].

The top part of Fig. 4 displays the calculated adsorption geometries for Au_4 and Au_{13} on TiC(0 0 1) [17–19]. Au_4 and Au_{13} are models for the 2D and 3D clusters of Au seen in STM [18,19]. A Bader analysis [45] of the electron density [17] showed a very small net charge transfer from the surface to the gold clusters (Q_{Au} < 0.2e). The bottom part of Fig. 4 displays electron-polarization function (ELF) [44] plots for Au_4 and Au_{13} on TiC(0 0 1). In the case of Au_4/TiC(0 0 1), there is a substantial concentration of electrons in the region outside the Au_4 unit. A similar phenomenon was observed for Au, Au_2 and other small clusters containing one layer of gold in contact with the carbide substrate [17]. In the Au_{13}/TiC(0 0 1) system, the Au cluster has two layers, and for the second layer the polarization of electrons is not as pronounced as seen in the case of Au_4/TiC(0 0 1). In fact, the polarization is yet only slightly noticeable in the first layer. The DF results in Fig. 4 are consistent with the photoemission results in Fig. 2. Theory and experiment show strong electronic perturbations for small

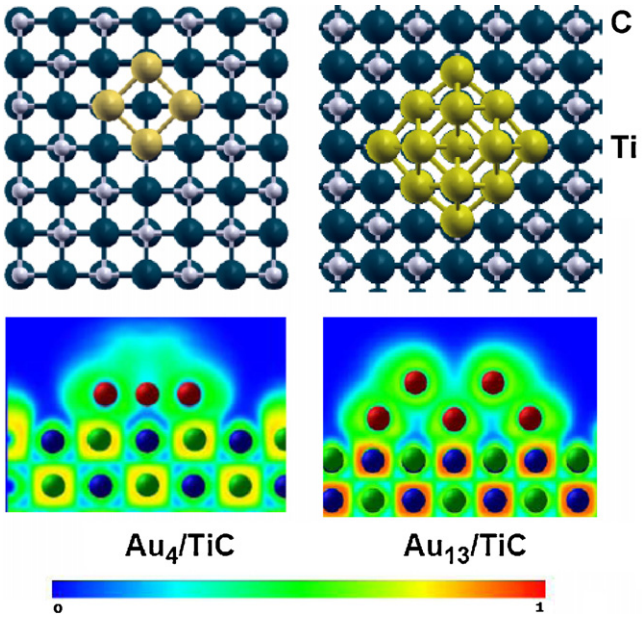

Fig. 4. *Top*: Calculated adsorption geometries for Au_4 and Au_{13} on TiC(0 0 1) [17–19]. The Au_{13} cluster consists of nine atoms in its first layer, in contact with the carbide substrate, and four atoms in its second layer. The Au atoms in the first layer are adsorbed on C sites. Web color code: Blue spheres denote Ti atoms, while white spheres represent C atoms. Gold is shown as dark yellow spheres. *Bottom*: ELF maps for Au_4 and Au_{13} on TiC(0 0 1) [17–19]. On the right side is shown a cut along the diagonal of the Au_{13} cluster in a plane which contains 5 gold atoms. The probability of finding the electron varies from 0 (blue color in the web) to 1 (red color in the web).

Au clusters in contact with TiC(0 0 1). On the basis of the charge polarization induced by the carbide substrate, one can expect big differences between the chemical reactivity of 2D and 3D gold clusters [17–19].

3.2. CO oxidation on Au/TiC(0 0 1)

Au nanoparticles dispersed on TiC films can oxidize carbon monoxide ($2CO + O_2 \rightarrow 2CO_2$) at temperatures below 200 K [16,46]. DF calculations indicate that CO does not interact with free Au_2 or Au_4 but has bonding energies of −1.13 eV on Au_2/TiC(0 0 1) and −0.90 eV on Au_4/TiC(0 0 1) [17]. Furthermore, the bonding energy of CO on pure TiC(0 0 1), −0.75 eV, is also smaller than those on the Au/TiC systems. Gold also affects the reactivity of O_2 on TiC(0 0 1) [20]. DF calculations give an O_2 adsorption energy of only −0.45 eV on TiC(0 0 1), but our model calculations [20] show that it increases to −1.41 eV on Au_4/TiC(0 0 1). O_2 binds to Au_4/TiC(0 0 1) with its O–O bond parallel to the surface (see Fig. 5). The O–O distance increases from 1.23 Å in free O_2 to 1.55 Å in adsorbed O_2. Although there is not a total cleavage of the O–O bond, the O_2 molecule has been activated by the Au/TiC(0 0 1) surface and is ready to react with CO.

In experiments of photoemission and thermal-desorption spectroscopy, we study the adsorption of O_2 on Au/TiC(0 0 1) and the subsequent oxidation of CO [20]. After dosing molecular oxygen to a TiC(0 0 1) surface pre-covered with 0.2 ML of Au at 150 K, the corresponding O 1s spectrum was dominated by a peak at ~531.8 eV, which corresponds to adsorbed O_2 [20]. There was also an O_2-induced shift of ~0.7 eV in the binding energy of the Au $4f_{7/2}$ peak, implying direct Au–O_2 bonding interactions. In a set of experiments, 0.3 L of O_2 were dosed to the Au/TiC(0 0 1) surface at 150 K. The sample containing chemisorbed O_2 was cooled down to 100 K, exposed to 0.6 L of CO, and the evolution of CO_2 was monitored with a mass spectrometer while increasing the sample temperature

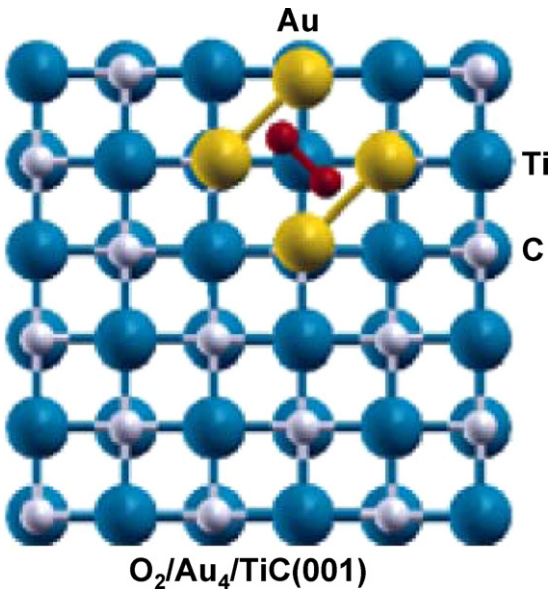

Fig. 5. Geometry calculated for the adsorption of O_2 on a Au_4 cluster supported on TiC(0 0 1). O_2 is adsorbed with its molecular axis parallel to the Au_4/TiC(0 0 1) surface [20]. Web color code: Blue spheres, Ti atoms; small white spheres, C atoms; dark yellow spheres, Au atoms; small red spheres, O atoms.

from 100 to 300 K. Desorption of CO_2 was observed at temperatures between 140 and 160 K. Thus, it appears that the oxygen species active during the low-temperature oxidation of carbon monoxide on Au/TiC(0 0 1) is chemisorbed O_2, as occurs in the case of Au/oxide surfaces [26,29].

The polarization of charge seen for Au_4 on TiC(0 0 1), bottom of Fig. 4, should facilitate bonding of the adatoms with electron-acceptor molecules (CO, O_2, C_2H_4, SO_2, thiophene, etc.) [17] and helps to explain the high chemical activity that Au/TiC exhibits for the oxidation of CO [16,20], DeSOx [18], and hydrodesulfurization reactions [19].

3.3. *Dissociation of SO_2 on Au/TiC(0 0 1)*

The destruction of SO_2 (DeSOx) is a very important problem in environmental chemistry due to the negative effects of acid rain (main product of the oxidation of SO_2 in the atmosphere) on the ecology and corrosion of monuments or buildings [48,49]. The top panel in Fig. 6 shows S 2p spectra collected after dosing SO_2 at 300 K to clean TiC(0 0 1) and a carbide surface pre-covered with 0.2 ML of Au [18]. On TiC(0 0 1) some dissociative chemisorption, $SO_2(gas) \rightarrow S(ads) + 2O(ads)$, occurs and a typical doublet for adsorbed atomic sulfur is seen from 161 to 163.5 eV [7]. In general terms, TiC(0 0 1) can be classified as a poor DeSOx system [7]. Au(1 1 1) and polycrystalline gold also interact weakly with SO_2 and are not efficient for the dissociation of S–O bonds [50]. However, after depositing Au nanoparticles on TiC(0 0 1) there is a drastic increase in the reactivity of the system. The S 2p spectrum recorded after dosing SO_2 to Au/TiC(0 0 1) shows a clear enhancement in the uptake of sulfur with respect to clean TiC(0 0 1). Even more important, photoemission results indicate that there is a full dissociation of SO_2 on Au/TiC(0 0 1) at 150 K [18], while only chemisorbed SO_2 is observed on TiC(0 0 1) at the same temperature [7].

The photoemission data reveals that Au/TiC(0 0 1) is a much better DeSOx system than either Au/MgO(1 0 0) or Au/TiO_2(1 1 0) [18]. Au particles dispersed on MgO(1 0 0) are able to perform the oxidation of CO [29] and bind SO_2 stronger than extended surfaces of gold [50], but the Au/MgO(1 0 0) system is not able to dissociate the SO_2 molecule which desorbs intact when raising the temperature

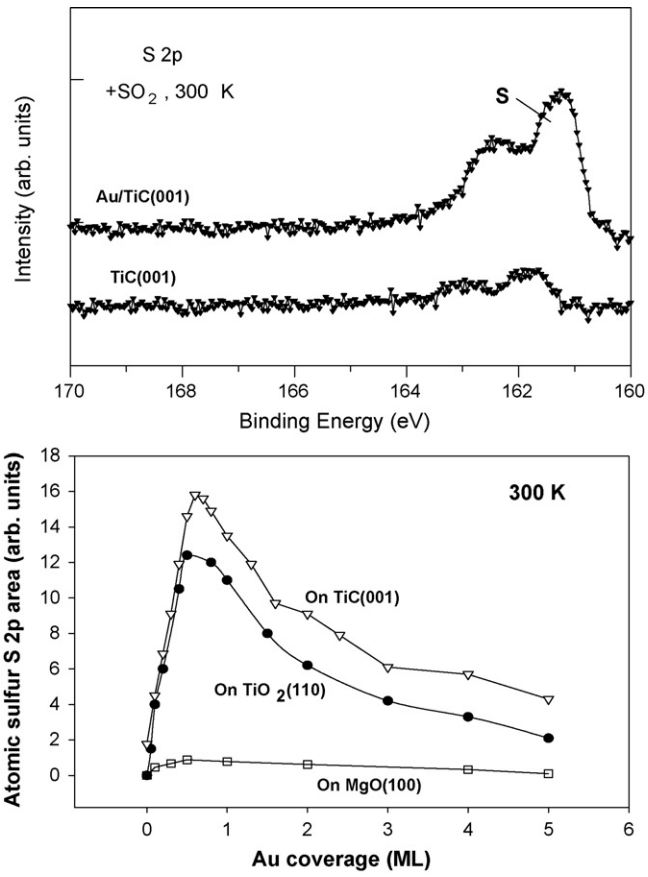

Fig. 6. *Top*: S 2p spectra collected after dosing 5 L of SO_2 at 300 K to TiC(0 0 1) and to a surface pre-covered with 0.2 ML of gold. The position of the S 2p features denotes the presence of atomic sulfur on the surfaces [18]. A photon energy of 380 eV was used to excite the electrons. *Bottom*: Effect of Au coverage on the amount of atomic S deposited on Au/MgO(0 0 1) [51], Au/TiO_2(1 1 0) [52], and Au/TiC(0 0 1) [18] after dosing 5 L of SO_2 at 300 K.

from 150 to 270 K [51]. In the case of Au particles supported on TiO_2(0 0 1), SO_2 adsorbs molecularly at 150 K and dissociate upon heating to room temperature [52]. Au/TiC(0 0 1) is able to break both S–O bonds at a temperature as low as 150 K [18]. The bottom panel in Fig. 6 compares the amount of atomic sulfur adsorbed after exposing Au/MgO(1 0 0) [51], Au/TiO_2(1 1 0) [52] and Au/TiC(0 0 1) [18] to 5 L of SO_2 at 300 K. Under these conditions the amount of SO_2 that dissociates on Au/MgO(1 0 0) is negligible [51]. The deposition of Au on TiO_2(1 1 0) produces surfaces quite active for the destruction of SO_2 at 300 K [51]. In Fig. 6, Au/TiC(0 0 1) displays a higher DeSOx activity than Au/TiO_2(1 1 0) even at big Au loads. Images of STM for Au/TiC(0 0 1) point to a very high DeSOx activity when the average particle height is smaller than 0.5 nm. The DeSOx activity of Au/TiC(0 0 1) decreases substantially when the particle height goes above 1 nm at Au coverages higher than 1 ML. Small Au clusters are essential for a high DeSOx activity.

Fig. 7 shows the calculated adsorption energy for SO_2 on clean TiC(0 0 1) and on carbide surfaces with Au atoms, Au_4 or Au_{13} clusters, a Au wire, and a flat Au monolayer [18]. All the Au/TiC(0 0 1) surfaces bond SO_2 stronger than clean TiC(0 0 1) [7] or the corresponding isolated Au system. Spontaneous dissociation was observed when the SO_2 was set at gold–carbide interfaces. Thus, supported Au atoms, Au_4, Au_{13} and a Au wire worked in a cooperative way with the carbide and dissociated S–O bonds. Photoemission results for the SO_2/Au/TiC(0 0 1) system also indicate the direct participation of Au, Ti and C sites in S–O bond cleavage [18]. In Fig. 7, an ideal flat monolayer of gold bonded to

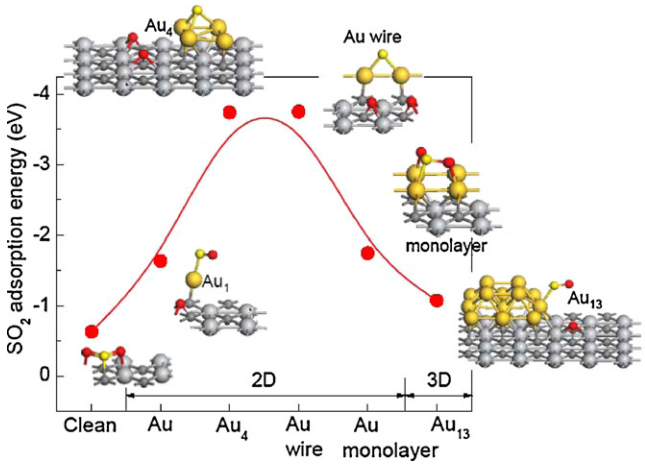

Fig. 7. Calculated adsorption energies (RPBE functional [42], DMol^3 code [41]) and bonding configurations for SO_2 on TiC(0 0 1) and Au/TiC(0 0 1) [7,18]. Au atoms, Au_4 and Au_{13} clusters, a Au wire, and a flat Au monolayer were deposited on TiC(0 0 1) [17,18]. The SO_2 was initially set at the gold/carbide interface and, in most cases, spontaneously dissociated during geometry optimization [18]. Web color code: Au is shown as big yellow spheres, Ti as big grey spheres, C as small grey spheres, S as small yellow spheres, and O as small red spheres.

TiC(0 0 1) adsorbs SO_2 much stronger than Au(1 1 1) or Au(1 0 0), but it is not able to dissociate the adsorbate due to the lack of a gold–carbide interface. The DF calculations corroborate that the size of the Au particle has a drastic effect on the reactivity of the system. Supported Au_{29} displayed a much lower DeSOx activity than supported Au_4 or Au_{13} and no dissociation of SO_2 was observed [18]. The effects of the Au ↔ TiC(0 0 1) interactions were significant only when one had small Au particles.

3.4. Hydrodesulfurization of thiophene on Au/TiC(0 0 1)

Hydrodesulfurization (HDS) is one of the largest processes in petroleum refineries where sulfur is removed from the crude oil [53]. Sulfur-containing compounds are converted to H_2S and hydrocarbons by reaction with hydrogen over a catalyst. The current HDS catalysts, mixtures of MoS_2 and Ni or Co, cannot provide fuels with the low content of sulfur required by new environmental regulations [8,15]. The search for better desulfurization catalysts is a major issue nowadays in the oil industry and academic institutions [8,15,53]. One option involves the use of metal carbides as catalysts precursors [6,8,12,15].

Thiophene is a typical test molecule in HDS studies [10,15,53,54]. The aromatic ring in thiophene makes its C–S bonds quite stable [19,54], and for this molecule the desulfurization reactions are much more difficult than those for other sulfur containing molecules such as thiols or SO_2 [15,53]. Thiophene adsorbs molecularly on TiC(0 0 1) at 100 K and desorbs intact upon heating the surface to 200 K [19]. The top panel in Fig. 8 displays S 2p spectra recorded after dosing a small amount of thiophene at 100 K to a TiC(0 0 1) surface pre-covered with 0.2 ML of Au [19]. The positions of the S 2p features indicate that thiophene does not decompose on the Au/TiC(0 0 1) surface, but the adsorption bond is substantially stronger than on TiC(0 0 1). Molecules of thiophene (∼0.13 ML) are bonded to the Au/TiC(0 0 1) at 300 K, and complete desorption is only seen after heating to 450 K. After saturating this Au/TiC(0 0 1) surface with thiophene at 100 K (4 L exposure), a TDS spectrum showed multilayer desorption at ∼135 K and monolayer desorption from 150 to 450 K [19]. This indicates an increase of 0.45–0.65 eV in the adsorption energy of thiophene with respect to those on TiC(0 0 1) and Au(1 1 1). The strength of the Au ↔ C_4H_4S interactions depends strongly on the amount of gold deposited

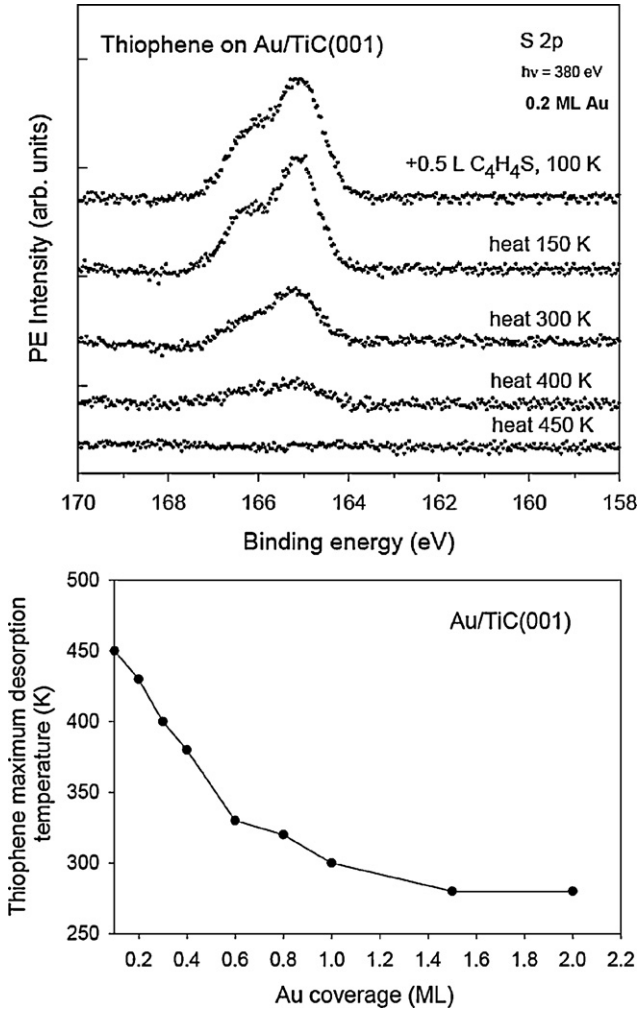

Fig. 8. *Top panel*: S 2p core level spectra for the adsorption of thiophene on a TiC(0 0 1) surface pre-covered with 0.2 ML of Au. The dosing of thiophene was carried at 150 K and the sample was then heated to the indicated temperatures [19]. A photon energy of 380 eV was used to acquire the S 2p spectra. *Bottom panel*: Maximum thiophene desorption temperature from Au/TiC(0 0 1) as a function of gold coverage. From clean TiC(0 0 1), thiophene desorbs at temperatures below 200 K [19].

on the carbide substrate, bottom panel of Fig. 8. At very small coverages of Au (∼0.1 ML), thiophene remained on the surface up to 450 K. On the other hand, at Au coverages above 1.5 ML, the maximum thiophene desorption temperature was 280 K. This trend reflects variations in the height and size of the Au particles (Fig. 1): a large thiophene bonding energy is seen on small 2D Au particles which expose sites directly in contact with the TiC(0 0 1) substrate and exhibit a charge polarization (Fig. 4) that facilitates interactions of the adatoms with electron-acceptor molecules [17].

Fig. 9 shows the calculated geometries for thiophene adsorbed on Au_4 and Au_{29} clusters supported on TiC(0 0 1) [19]. In the case of unsupported C_4H_4S–Au_4 the bonding energy of thiophene was ∼−1 eV (DMol^3 calculation, RPBE functional) and the molecule was attached to the metal cluster in a η^5 conformation. A similar bonding conformation was found on Au_4/TiC(0 0 1), see Fig. 9, with the bonding energy of thiophene increasing to ∼−2 eV. This bonding energy is much larger than the value of −0.1 eV found for thiophene on clean TiC(0 0 1) where the molecule binds via its S lone-pair [19]. Furthermore, in Fig. 9, one can see a large distortion in the geometry of thiophene after adsorbing the molecule on Au_4/TiC(0 0 1). In gas phase, the calculated C–S bond distances in thiophene were 1.746 Å. Upon adsorption on Au_4/TiC(0 0 1), the C–S

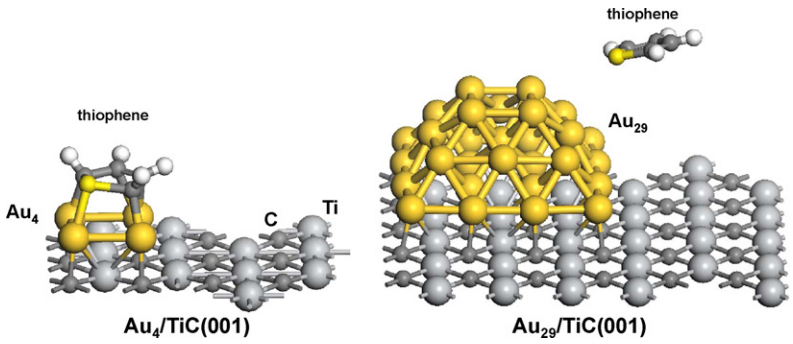

Fig. 9. Calculated adsorption geometries for thiophene on Au_4/TiC(0 0 1) and Au_{29}/TiC(0 0 1). In general, thiophene can bind to a surface via its S lone-pair (η^1 coordination mode) or through the aromatic ring of the molecule (η^5 coordination mode) [19,54]. Thiophene is bonded to the Au_4 cluster through its aromatic ring (η^5 coordination), and interacts with the Au_{29} cluster through its S lone-pair (η^1 coordination). On clean TiC(0 0 1), thiophene bonds via its S lone-pair (η^1 coordination) [19].

bond distances increased to an average value of ~1.93 Å. The LUMO of thiophene, $3b_1$ orbital, is C–S antibonding [54]. The polarization of electrons seen in Fig. 4 for Au_4/TiC(0 0 1) facilitates a transfer of charge from gold to the LUMO of thiophene which induces a quite large elongation (~0.2 Å) in the C–S bonds. Although the C–S bonds of thiophene are significantly weaken on Au_4/TiC(0 0 1), they do not dissociate spontaneously. For the interaction of thiophene with Au_{29}/TiC(0 0 1) the bonding energy of the molecule was only −0.15 eV. The gold atoms in Au_{29}/TiC(0 0 1) do not undergo the charge polarization seen for Au_4/TiC(0 0 1) [17–19] and, thus, exhibit weak bonding interactions with thiophene.

In the UHV experiments of Fig. 8, there was no cleavage of the C–S bonds when thiophene was dosed to Au/TiC(0 0 1) [19]. In HDS processes, H adatoms present in the surface of the catalyst can help in the cleavage of the C–S bonds of thiophene [53,54]. Gold nanoparticles supported on TiC(0 0 1) are able to dissociate the H_2 molecule [19], as expected [55], yielding the H atoms necessary for the hydrogenolysis of C–S bonds. The catalytic activity of Au/TiC(0 0 1) for the HDS of thiophene was tested at 600 K [19]. A TiC(0 0 1) surface with 0.2 ML of Au was set in a batch reactor (1 Torr of thiophene, 500 Torr of H_2, 90 min reaction time), and the total amount of C_4 hydrocarbons formed was determined using gas chromatography. Under the reaction conditions investigated, TiC(0 0 1) displayed negligible catalytic activity. Fig. 10 compares the thiophene HDS activities measured for Mo(1 1 0) [56], a conventional Ni/MoS_x catalyst [57], TiC(0 0 1) [19], and Au/TiC(0 0 1)

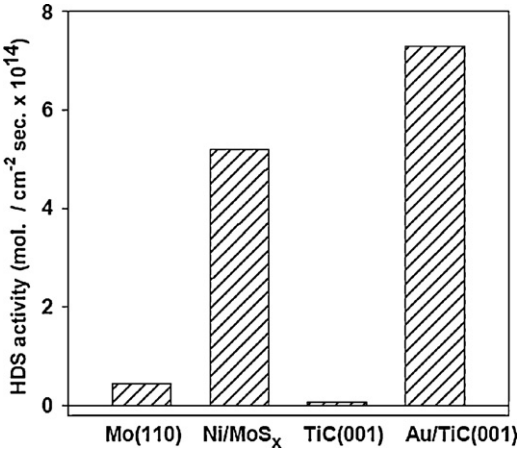

Fig. 10. Thiophene HDS activities for Mo(1 1 0) [56], a Ni/MoS_x catalyst [57], TiC(0 0 1) [19], and Au/TiC(0 0 1) [19]. The coverage of gold on TiC(0 0 1) was 0.2 ML. In the *y*-axis is plotted the total amount of C_4 hydrocarbons formed during the HDS of thiophene (1 Torr of thiophene, 500 Torr of H_2, 600 K, 90 min reaction time) [19,58]. The number of C_4 hydrocarbon molecules produced was normalized by the reaction time and the exposed surface area of each sample.

[19]. The HDS activity found for Mo(1 1 0) is comparable to that seen in a previous study [58]. Similar HDS activities were observed for Mo(1 1 1) and Mo(1 0 0) surfaces [58]. The Mo surfaces are not good HDS catalysts because they interact too strongly with the sulfur produced after the cleavage of the C–S bonds in thiophene [56]. Many industrial HDS catalysts contain a mixture of molybdenum sulfide promoted with Ni on a γ-alumina support [53]. The conventional Ni/MoS_x catalyst binds thiophene well [57] without being deactivated by the S atoms produced in the HDS process. In spite of the very poor desulfurization performance of TiC(0 0 1), the Au/TiC(0 0 1) system displays an HDS activity higher than that of Ni/MoS_x [19]. The small Au nanoparticles probably increase the HDS activity of TiC by enhancing the adsorption energy of thiophene and by helping in the dissociation of H_2 to produce the hydrogen necessary for the hydrogenolysis of C–S bonds and the removal of sulfur [19]. The importance of H adatoms in the HDS process is well established [59,60]. DF calculations indicate that essentially there is no energy barrier for the dissociation of H_2 on Au_4/TiC(0 0 1) [19].

The results discussed in Sections 3.2–3.4 indicate that the electronic perturbations induced by titanium carbide on gold have a strong impact on the chemical reactivity of the noble metal for CO oxidation, DeSOx and hydrodesulfurization. In preliminary experiments we also have found that the Au ↔ TiC interactions make Au/TiC(0 0 1) a good catalyst for the reduction of NO and the water-gas shift reaction. For several of these reactions, the Au/TiC system is more chemically active than systems generated by depositing Au nanoparticles on oxide surfaces [18–20]. Furthermore, titanium carbide may not be the only carbide useful for enhancing the chemical reactivity of gold [61]. After examining the behavior of Au on several metal carbides with DF calculations [61], one finds that the electronic perturbations on Au substantially increase when going from TiC to ZrC or TaC as a support. Au/ZrC(0 0 1) and Au/TaC(0 0 1) have the properties necessary for being very good catalysts for CO oxidation and HDS reactions [61].

4. Summary and conclusions

We have reviewed recent articles [16–20] which show the excellent performance reported for novel Au–TiC catalysts. High-resolution photoemission, STM, and DF periodic calculations were used to study the adsorption of gold on a TiC(0 0 1) surface. Gold grows forming 2D (very low coverages) and 3D (medium and large coverages) islands on the carbide substrate. A positive shift in the binding energy of the C 1s core level is observed after the deposition of Au on TiC(0 0 1). The results of the density-functional calculations corroborate the formation of Au–C bonds. In general, the bond between Au and the TiC(0 0 1) surface exhibits very little ionic character, but there is a substantial polarization of electrons around Au that affects its chemical properties.

After coadsorbing O_2 and CO on Au/TiC(0 0 1) at 100 K, evolution of CO_2 was observed at temperatures between 140 and 160 K. The oxygen species active during the low-temperature oxidation of carbon monoxide on Au/TiC(0 0 1) is chemisorbed O_2. DF calculations give an O_2 adsorption energy of only −0.45 eV on TiC(0 0 1), but it substantially raises to −1.41 eV on Au_4/TiC(0 0 1). The O–O distance increases from 1.23 Å in free O_2 to 1.55 Å for O_2 adsorbed on Au_4/TiC(0 0 1). Although there is not a complete cleavage of the O–O bond, the O_2 molecule has been activated by the Au/TiC(0 0 1) surface and is ready to react with CO.

At temperatures below 200 K, Au/TiC(0 0 1) is able to perform the full decomposition of SO_2. Photoemission results indicate the direct participation of Au, Ti and C sites in S–O bond cleavage. The size of the Au particles has a drastic effect on the DeSOx activity of a Au/TiC(0 0 1) surface. Images of STM point to a very high DeSOx activity when the average particle height is smaller than 0.5 nm. The DeSOx activity of Au/TiC(0 0 1) decreases substantially when the particle height goes above 1 nm at Au coverages higher than 1 ML. Small 2D gold clusters are essential for a high DeSOx activity. Au/TiC(0 0 1) is a much better DeSOx system than either Au/MgO(1 0 0) or Au/TiO_2(1 1 0).

Au nanoparticles drastically increase the hydrodesulfurization activity of TiC(0 0 1) by enhancing the bonding energy of thiophene and by helping in the dissociation of H_2 to produce the hydrogen necessary for the hydrogenolysis of C–S bonds and the removal of sulfur. H_2 spontaneously dissociates on small two-dimensional clusters of gold in contact with TiC(0 0 1). On these systems, the adsorption energy of thiophene is 0.45–0.65 eV larger than on TiC(0 0 1) or Au(1 1 1). Thiophene binds in a η^5 configuration with a large elongation (∼0.2 Å) of the C–S bonds.

Acknowledgements

The authors are grateful to B. Roldán-Cuenya (University of Central Florida) and J. Gomes (Universidade do Porto) for thought-provoking discussions about the properties of Au/TiC. Many thanks to T. Jirsak (BNL) for his help with the operation of the U7A beamline and the photoemission experiments at the NSLS. The research carried out at BNL was supported by the US Department of Energy, Chemical Sciences Division. J.A.R. acknowledges the support of the *Generalitat de Catalunya* (grant 2006PIV00009) in a visit to the Universitat de Barcelona. F.V. thanks the Spanish Ministry of Education and Science and Universitat de Barcelona for supporting his pre-doctoral research. K. N. is grateful to the Nippon Foundation for Materials Science for grants that made possible part of this work and F.I. acknowledges financial support from Spanish MICINN grant FIS2008-02238/FIS. Computational time on the Center for Functional Nanomaterials at BNL and on the *Marenostrum* supercomputer of the Barcelona Supercomputing Center is gratefully acknowledged.

References

[1] H.H. Hwu, J.G. Chen, Chem. Rev. 105 (2005) 185.
[2] P. Liu, J.A. Rodriguez, J. Chem. Phys. 120 (2004) 5414.
[3] R.B. Levy, M. Boudart, Science 181 (1973) 547.
[4] J.B. Claridge, A.P.E. York, A.J. Brungs, C. Marquez-Alvarez, J. Sloan, S.C. Tsang, M.L.H. Green, J. Catal. 180 (1998) 85.
[5] A.J. Brungs, A.P.E. York, M.L.H. Green, Catal. Lett. 57 (1999) 65.
[6] R.R. Chianelli, G. Berhault, Catal. Today 53 (1999) 357.
[7] J.A. Rodriguez, P. Liu, J. Dvorak, T. Jirsak, J. Gomes, Y. Takahashi, K. Nakamura, Surf. Sci. 543 (2003) L675.
[8] S.T. Oyama, Catal. Today 15 (1992) 179.
[9] J.A. Rodriguez, J. Dvorak, T. Jirsak, J. Phys. Chem. B 104 (2000) 11515.
[10] T.P. Clair St., S.T. Oyama, D.F. Cox, Surf. Sci. 511 (2002) 294.
[11] P. Liu, J.A. Rodriguez, J. Chem. Phys. 119 (2003) 10895.
[12] B. Diaz, S.J. Sawhill, D.H. Bale, R. Main, D.C. Phillips, S. Korlann, R. Self, M.E. Bussell, Catal. Today 86 (2003) 191.
[13] V. Schwartz, V.T. da Silva, S.T. Oyama, J. Mol. Catal. A 163 (2000) 251.
[14] P. Liu, J.A. Rodriguez, T. Asakura, J. Gomes, K. Nakamura, J. Phys. Chem. B 109 (2005) 4575.
[15] E. Furimsky, Appl. Catal. A: Gen. 240 (2003) 1.
[16] L.K. Ono, B. Roldán-Cuenya, Catal. Lett. 113 (2007) 86.
[17] J.A. Rodriguez, F. Viñes, F. Illas, P. Liu, Y. Takahashi, K. Nakamura, J. Chem. Phys. 127 (2007) 211102.
[18] J.A. Rodriguez, P. Liu, F. Viñes, F. Illas, Y. Takahashi, K. Nakamura, Angew. Chem. Int. Ed. 47 (2008) 6685.
[19] J.A. Rodriguez, P. Liu, F. Viñes, F. Illas, Y. Takahashi, K. Nakamura, J. Am. Chem. Soc. 131 (2009) 8592.
[20] J.A. Rodriguez, L. Feria, T. Jirsak, Y. Takahashi, K. Nakamura, F. Illas, J. Am. Chem. Soc. 132 (2010) 3177.
[21] J.M. Thomas, W.J. Thomas, Principles and Practice of Heterogeneous Catalysis, VCH, New York, 1997.
[22] B. Hammer, J.K. Nørskov, Nature 376 (1995) 238.
[23] J.A. Rodriguez, Dekker Encyclopedia of Nanoscience and Nanotechnology, Dekker, New York, 2004, pp. 1297–1304.
[24] M. Haruta, Catal. Today 36 (1997) 153.
[25] M.S. Chen, D.W. Goodman, Science 306 (2004) 252.
[26] N. Cruz Hernárdez, J.F. Sanz, J.A. Rodriguez, J. Am. Chem. Soc. 128 (2006) 15600.
[27] A. Vijay, G. Mills, H. Metiu, J. Chem. Phys. 118 (2003) 6536.
[28] C.T. Campbell, S.C. Parker, D.E. Starr, Science 298 (2002) 811.
[29] L.M. Molina, B. Hammer, Appl. Catal. A: Gen. 291 (2005) 21.
[30] M. Boronat, P. Concepción, A. Corma, S. González, F. Illas, P. Serna, J. Am. Chem. Soc. 129 (2007) 16230.
[31] L.E. Toth, Transition Metal Carbides and Nitrides, vol. 7 of Refractory Materials, Academic, New York, 1971.
[32] E.K. Storms, The Refractory Carbides, Academic, New York, 1967.
[33] F. Viñes, C. Sousa, P. Liu, J.A. Rodriguez, F. Illas, J. Chem. Phys. 122 (2005) 174709.
[34] J.A. Rodriguez, P. Liu, J. Dvorak, T. Jirsak, J. Gomes, Y. Takahashi, K. Nakamura, J. Chem. Phys. 121 (2004) 465.
[35] J.A. Rodriguez, P. Liu, J. Dvorak, T. Jirsak, J. Gomes, Y. Takahashi, K. Nakamura, Phys. Rev. B 69 (2004) 115414.
[36] F. Viñes, C. Sousa, F. Illas, P. Liu, J.A. Rodriguez, J. Phys. Chem. C 111 (2007) 16982.
[37] Y.F. Zhang, F. Viñes, Y.J. Xu, Y. Li, J.Q. Li, F. Illas, J. Phys. Chem. B 110 (2006) 15454.
[38] P. Frantz, S.V. Didziulis, Surf. Sci. 412/413 (1998) 384.
[39] P. Frantz, S.V. Didziulis, P.B. Merril, S.S. Perry, O. El-bjerami, S. Imaduddin, J. Phys. Chem. B 103 (1999) 11129.
[40] G. Kresse, J. Furthmüller, Comput. Mater. Sci. 6 (1996) 15;
G. Kresse, J. Furthmüller, Phys. Rev. B 54 (1996) 11169.
[41] B. Delley, J. Chem. Phys. 92 (1990) 508;
B. Delley, J. Chem. Phys. 113 (2000) 7756.
[42] B. Hammer, L.B. Hansen, J.K. Nørskov, Phys. Rev. B 59 (1999) 7413.
[43] J.P. Perdew, J.A. Chevary, S.H. Vosko, K.A. Jackson, M.R. Pederson, D.J. Singh, C. Fiolhais, Phys. Rev. B 46 (1992) 6671.
[44] B. Silvi, A. Savin, Nature 371 (1994) 683.
[45] R.F.W. Bader, Atoms in Molecules: A Quantum Theory, Oxford Science, Oxford, UK, 1990.
[46] L.K. Ono, D. Sudfeld, B. Roldan Cuenya, Surf. Sci. 600 (2006) 5041.
[47] A. Naitabdi, L.K. Ono, B. Roldan Cuenya, Appl. Phys. Lett. 89 (2006) 043101.
[48] A.C. Stern, R.W. Boubel, D.B. Turner, D.L. Fox, Fundamentals of Air Pollution, 2nd ed., Academic, Orlando, USA, 1984.
[49] A. Pieplu, O. Saur, J.-C. Lavalley, O. Legendre, C. Nedez, Catal. Rev. -Sci. Eng. 40 (1998) 409.
[50] G. Liu, J.A. Rodriguez, J. Dvorak, J. Hrbek, T. Jirsak, Surf. Sci. 505 (2002) 295.
[51] J.A. Rodriguez, M. Pérez, T. Jirsak, J. Evans, J. Hrbek, L. González, Chem. Phys. Lett. 378 (2003) 526.
[52] J.A. Rodriguez, G. Liu, T. Jirsak, J. Hrbek, Z. Chang, J. Dvorak, A. Maiti, J. Am. Chem. Soc. 124 (2002) 5242.
[53] H. Topsøe, B.S. Clausen, F.E. Massoth, Hydrotreating Catalysis, Springer-Verlag, New York, 1996.
[54] J.A. Rodriguez, J. Phys. Chem. B 101 (1997) 7524.
[55] A. Corma, M. Boronat, S. González, F. Illas, Chem. Commun. (2007) 3371.
[56] J.A. Rodriguez, J. Dvorak, T. Jirsak, Surf. Sci. 457 (2000) L413.
[57] J.A. Rodriguez, J. Dvorak, A.T. Capitano, A.M. Gabelnick, J.L. Gland, Surf. Sci. 429 (1999) L462.
[58] M.E. Bussell, A.J. Gellman, G.A. Somorjai, J. Catal. 110 (1988) 423.
[59] S.T. Oyama, T. Gott, K. Asakura, S. Takakusagi, K. Miyazaki, Y. Koike, K.K. Bando, J. Catal. 268 (2009) 209.
[60] N.A. Khan, H.H. Hwu, J.G. Chen, J. Catal. 205 (2002) 259.
[61] E. Florez, F. Viñes, J.A. Rodriguez, F. Illas, J. Chem. Phys. 130 (2009) 244706.